J. Fluid Mech. (1988), *vol.* 188, *pp.* 491–508
Printed in Great Britain

Surface waves of large amplitude beneath an elastic sheet. Part 2. Galerkin solution

By LAWRENCE K. FORBES
Department of Mathematics, University of Queensland,
St Lucia 4067, Queensland, Australia

(Received 17 July 1986 and in revised form 24 August 1987)

This study continues the work of Forbes (1986) on periodic waves beneath an elastic sheet floating on the surface of an infinitely deep fluid. The solution is sought as a Fourier series with coefficients that are computed numerically. Waves of extremely large amplitude are found to exist, and results are presented for waves belonging to several different nonlinear solution branches, characterized by different numbers of inflexion points in the wave profiles. The existence of multiple solutions, conjectured in the previous paper (Forbes 1986), is confirmed here by direct numerical computation.

1. Introduction

This paper is concerned with the form of finite-amplitude surface waves in the presence of a floating elastic sheet. The work presented here represents a direct continuation of the study begun by Forbes (1986, referred to hereinafter as Paper 1). In this earlier work it was explained that a motivation for investigating such a problem was to describe the properties of waves beneath a floating ice sheet and references are given there to work involving ice. The results to be given in the present paper, however, will show that such a model is probably of only limited relevance to ice, although it doubtless can be applied successfully to floating sheets of different composition.

The computation of surface waves of large amplitude is an important problem in fluid mechanics and has a long history. Many of the contributions to this problem are summarized in a recent review article by Schwartz & Fenton (1982). Early work, such as Stokes' (1880) investigation of gravity waves and Wilton's (1915) study of capillary–gravity waves, typically relied upon Fourier series and perturbation expansions to obtain approximate solutions to the nonlinear equations describing the shape of periodic waves. More recently, the digital computer has been used to automate the process of obtaining such series solutions. Thus Schwartz (1974) modified Stokes' series for the pure gravity wave and computed solutions with wave height very close to the theoretical maximum, at which a cusp enclosing an angle of 120° is formed at the crest. Wilton's series for the capillary–gravity wave have been extended by Hogan (1980, 1981). Holyer (1979) has used similar techniques to solve the problem of waves at an interface, and a series solution for waves beneath an elastic plate was presented in Paper 1.

Purely numerical solutions to surface-wave problems have also been undertaken. Schwartz & Vanden-Broeck (1979), for example, obtained accurate solutions for the capillary–gravity-wave problem using an integral equation formulated in an inverse plane in which the velocity potential and stream function were chosen as independent

variables. A method based on the use of Fourier series in the plane of the physical variables was adopted by Rienecker & Fenton (1981), and Pullin & Grimshaw (1983) and Grimshaw & Pullin (1986) used a combination of Fourier-series and integral-equation techniques to investigate the properties of extreme interfacial waves.

In this paper we continue the study of periodic waves beneath a floating elastic sheet, using a Fourier-series solution in the inverse plane of the complex potential. Unlike Paper 1, however, in which the Fourier coefficients were developed as expansions in the wave height, they are here computed directly using a Newton–Raphson technique. The problem formulation and numerical solution algorithm are described in §§2 and 3. Results are presented in §4, and represent a summary of about 200 separate converged numerical solutions, obtained at the expense of many tens of hours of computing time on an IBM 3083E machine. This is by no means an exhaustive study, but it does permit certain trends in the behaviour of the solution to be identified. In Paper 1, it was found that the series-solution technique predicted singularities in the wave speed at quite modest values of the wave height, and these were interpreted as limitations of the physical model, perhaps indicating the need for a more complete description in which cracking of the elastic sheet could take place. The results in §4, however, show that this interpretation of the singularity predicted by the series method is incorrect; instead, it now appears that these singularities are associated with narrow regions of nonlinear resonance of the type described by Roberts (1981, 1983), and are indicative of multiple solutions. A summary in §5 concludes the paper.

2. Formulation

As in Paper 1, we consider periodic waves of length λ and speed c moving in a fluid of infinite depth and density ρ. An elastic sheet of thickness T, density ρ_{M} and flexural rigidity D floats on the surface of the fluid. The downward acceleration of gravity is g and the peak-to-trough wave height is $2A$. The waves are now viewed from a Cartesian coordinate system having the y-axis pointing vertically upward and moving with the waves such that a crest is permanently positioned at $x = 0$. Relative to this moving reference frame, the waves are stationary and the fluid flows in the positive x-direction.

The problem is now non-dimensionalized in the manner adopted by Schwartz & Vanden-Broeck (1979), by referring all lengths to $\lambda/2\pi$ and all velocities to $(g\lambda/2\pi)^{\frac{1}{2}}$. The elastic bending moment M of the sheet is scaled relative to the quantity $(\rho_{\mathrm{M}} g\lambda^3)(2\pi)^{-3}$ and the pressure P is referred to $\rho g\lambda/2\pi$.

Since the fluid beneath the elastic sheet is assumed to be ideal and to flow without rotation, it follows that a fluid-velocity potential ϕ and stream function ψ exist, satisfying the Cauchy–Riemann equations

$$u = \phi_x = \psi_y, \quad v = \phi_y = -\psi_x \tag{2.1}$$

within the fluid. The quantities u and v are respectively the x- and y-components of the fluid-velocity vector. At infinite depth,

$$u \to \mu^{\frac{1}{2}}, \quad v \to 0 \quad \text{as } y \to -\infty, \tag{2.2}$$

where the quantity $\mu = (2\pi c^2)(g\lambda)^{-1}$ is a dimensionless wave-speed parameter. In these non-dimensional coordinates, the waves are of length 2π and amplitude

$\alpha = 2\pi A/\lambda$, and a crest is located at $x = 0$; denoting the interface between the elastic sheet and the fluid as the line $y(x)$, it then follows that

$$y(0) - y(\pi) = 2\alpha. \tag{2.3}$$

The Bernoulli equation on the fluid surface $y(x)$ is written

$$\tfrac{1}{2}(u^2 + v^2) + y + P = \tfrac{1}{2}\mu + d_{\mathrm{M}} H, \tag{2.4}$$

in which $d_{\mathrm{M}} = \rho_{\mathrm{M}}/\rho$ is the ratio of the density of the elastic plate to the fluid density, and $H = 2\pi T/\lambda$ is the dimensionless thickness of the sheet.

The system of equations (2.1)–(2.4) is closed after specification of the pressure P. The classical theory of beams gives the relationship

$$P = d_{\mathrm{M}}\left[H - \frac{\mathrm{d}^2 M}{\mathrm{d}x^2}\right]. \tag{2.5}$$

In Paper 1 we derived the expression

$$M = -\frac{K\dfrac{\mathrm{d}^2 y}{\mathrm{d}x^2}}{\left[1 + \left(\dfrac{\mathrm{d}y}{\mathrm{d}x}\right)^2\right]^{\frac{3}{2}}} - \tfrac{1}{2}H\frac{\mathrm{d}^2 y}{\mathrm{d}x^2} \tag{2.6}$$

relating the elastic bending moment $M(x)$ to the vertical displacement $y(x)$ of the fluid–sheet interface. The parameter $K = (16\pi^4 D)(\rho_{\mathrm{M}} g \lambda^4)^{-1}$ is the non-dimensional flexural rigidity. Equation (2.6) allows for finite sheet thickness H, and does not require that the curvature of the fluid surface be small.

It follows from (2.1) that the complex potential $f = \phi + \mathrm{i}\psi$ is an analytic function of the variable $z = x + \mathrm{i}y$ within the fluid. The problem formulation is simplified by treating the complex potential f as the independent variable and seeking an analytic function $z(f)$ satisfying the equations of motion, since, as pointed out by Stokes (1880), the unknown surface location $y(x)$ maps simply to the streamline $\psi = 0$ in the f-plane. As suggested by Schwartz & Vanden-Broeck (1979), each complete wave cycle in the f-plane is now further mapped into a ζ-plane by the conformal transformation

$$f = \mathrm{i}\mu^{\frac{1}{2}} \ln \zeta,$$

and the new variable ζ is written $\zeta = r\mathrm{e}^{\mathrm{i}\theta}$. In the ζ-plane, each wave now occupies the disk $0 < r \leqslant 1$, $-\pi < \theta \leqslant \pi$, with the circle $r = 1$ corresponding to the fluid surface.

In the ζ-plane, the nonlinear equations (2.3)–(2.6) describing the surface shape transform to

$$y(1, 0) - y(1, \pi) = 2\alpha \tag{2.7}$$

and

$$\tfrac{1}{2}\mu\left(\frac{1}{x_\theta^2 + y_\theta^2} - 1\right) + y + P = d_{\mathrm{M}} H \quad \text{on } r = 1, \tag{2.8}$$

where the pressure is given by

$$P = d_{\mathrm{M}}\left(H - \frac{x_\theta M_{\theta\theta} - M_\theta x_{\theta\theta}}{x_\theta^3}\right) \quad \text{on } r = 1, \tag{2.9}$$

and the elastic bending moment is found from

$$M = \frac{K(x_\theta y_{\theta\theta} - y_\theta x_{\theta\theta})}{(x_\theta^2 + y_\theta^2)^{\frac{3}{2}} + \frac{1}{2}H(x_\theta y_{\theta\theta} - y_\theta x_{\theta\theta})} \quad \text{on } r = 1. \tag{2.10}$$

The solution thus consists of finding a function $z(\zeta)$ which is analytic in the disk $0 < r < 1$ and satisfies conditions (2.7)–(2.10) on the boundary $r = 1$. The wave-speed parameter μ is also unknown and is therefore to be determined.

3. The numerical solution

Solutions of period 2π are sought to the nonlinear equations of motion in §2 using the Fourier-series representation

$$z(\zeta) = \mathrm{i} \ln \zeta + \mathrm{i} \sum_{j=0}^{\infty} A_j \zeta^j, \tag{3.1}$$

in which the coefficients A_j, $j = 0, 1, 2, \ldots$ are all real, as in Paper 1. Equation (3.1) satisfies the fluid equations (2.1) and the condition (2.2) at infinite depth, and it therefore remains to choose the coefficients A_j, $j = 0, 1, 2, \ldots$ and the wave-speed parameter μ so as to satisfy the surface conditions (2.7)–(2.10).

We introduce Q evenly spaced numerical grid points $\theta_1, \theta_2, \ldots, \theta_Q$ at the fluid surface $r = 1$, separated by the interval $h = 2\pi(Q-1)^{-1}$. Here, $\theta_1 = -\pi$ and $\theta_Q = \pi$. The dependent variables $x(1, \theta)$ and $y(1, \theta)$ evaluated at the mesh points θ_k, $k = 1, 2, \ldots, Q$ are written as x_k and y_k, respectively, and their derivatives $x_\theta(1, \theta_k)$ and $y_\theta(1, \theta_k)$ are denoted as x'_k and y'_k, with similar notation for higher derivatives. The Fourier series (3.1) is truncated after the Nth-order term, so that its real and imaginary parts give approximately

$$\left.\begin{aligned} x_k &= -\theta_k - \sum_{j=1}^{N} A_j \sin(j\theta_k), \\ y_k &= A_0 + \sum_{j=1}^{N} A_j \cos(j\theta_k). \end{aligned}\right\} \tag{3.2}$$

The series (3.2) are differentiated exactly to give similar series expressions for x'_k, y'_k, x''_k, y''_k.

The elastic bending moment $M(\theta)$ is also computed approximately as a truncated Fourier series of the form

$$M(\theta_k) = M_0 + \sum_{j=1}^{N} M_j \cos(j\theta_k). \tag{3.3}$$

The coefficients $M_0, M_1, M_2, \ldots$ are given by the usual Euler formulae

$$\left.\begin{aligned} M_0 &= \frac{1}{2\pi} \int_{-\pi}^{\pi} M(\theta)\, \mathrm{d}\theta, \\ M_j &= \frac{1}{\pi} \int_{-\pi}^{\pi} M(\theta) \cos j\theta\, \mathrm{d}\theta, \quad j = 1, \ldots, N. \end{aligned}\right\} \tag{3.4}$$

Since the integrands in (3.4) are periodic functions of θ, the coefficients $M_0, M_1, \ldots, M_N$ may be evaluated to exponentially high-order accuracy using the trapezoidal

rule. Defining trapezoidal-rule weights $w_1 = w_Q = \frac{1}{2}h, w_k = h, k = 2, \ldots, Q-1$ and using (2.10), we have

$$M_j = \frac{K}{\gamma_j \pi} \sum_{k=1}^{Q} \frac{w_k(x'_k y''_k - y'_k x''_k)\cos(j\theta_k)}{(x'^2_k + y'^2_k)^{\frac{3}{2}} + \frac{1}{2}H(x'_k y''_k - y'_k x''_k)}, \quad j = 0, 1, 2, \ldots, N, \tag{3.5}$$

where the constant γ_j has the value 2 when $j = 0$ and 1 otherwise. Equation (3.3) is now differentiated to yield similar series for $M'(\theta_k)$ and $M''(\theta_k)$.

The Fourier series for the pressure $P(\theta)$ at the free surface is written approximately as

$$P(\theta_k) = P_0 + \sum_{j=1}^{N} P_j \cos(j\theta_k), \quad k = 1, 2, \ldots, Q, \tag{3.6}$$

and the Fourier coefficients $P_0, P_1, \ldots, P_N$ are obtained from (2.9) using the Euler formulae and the composite trapezoidal rule with weights $w_1, \ldots, w_Q$, as above. This gives

$$P_j = d_{\mathrm{M}} H \delta_j - \frac{d_{\mathrm{M}}}{\gamma_j \pi} \sum_{k=1}^{Q} \frac{w_k[x'_k M''(\theta_k) - M'(\theta_k) x''_k]\cos(j\theta_k)}{x'^3_k}, \quad j = 0, 1, \ldots, N, \tag{3.7}$$

in which the constant δ_j is either 1 when $j = 0$ or 0 for $j \neq 0$, and γ_j has the same values as in (3.5).

A damped Newton–Raphson method is now used to solve (2.7) and (2.8) for the vector $\boldsymbol{u} = [\mu, A_0, A_1, \ldots, A_N]^{\mathrm{T}}$ of the $N+2$ unknowns. We seek to solve an algebraic system of equations of the form

$$\boldsymbol{E}(\boldsymbol{u}) = \boldsymbol{0}, \tag{3.8}$$

where $\boldsymbol{E} = [E_0, E_1, \ldots, E_{N+1}]^{\mathrm{T}}$ is an error vector of length $N+2$, the individual elements of which are obtained as the discrete Fourier transforms of (2.7) and (2.8). For the first component of the error vector, (2.7) and (3.2) yield

$$E_0 = \sum_{l=0}^{[\frac{1}{2}(N-1)]} A_{2l+1} - \alpha \tag{3.9a}$$

and the notation $[\frac{1}{2}(N-1)]$ denotes the integer part of $\frac{1}{2}(N-1)$. The remaining components are obtained from (2.8) in the form

$$E_{j+1} = A_j + P_j - (\tfrac{1}{2}\mu + d_{\mathrm{M}} H)\,\delta_j + \frac{\mu}{2\gamma_j \pi} \sum_{k=1}^{Q} \frac{w_k \cos(j\theta_k)}{x'^2_k + y'^2_k}, \quad j = 0, 1, \ldots, N, \tag{3.9b}$$

where the constants γ_j, δ_j and weights w_k are as before.

To begin the computation, an initial guess is made for the vector $\boldsymbol{u}$; this is usually provided by the linearized solution

$$\left.\begin{aligned} \mu_0 &= 1 + d_{\mathrm{M}} K, \\ A_0^{(0)} &= 0, \\ A_1^{(0)} &= \alpha, \\ A_j^{(0)} &= 0, \quad j = 2, \ldots, N, \end{aligned}\right\} \tag{3.10}$$

given in Paper 1. The components of the error vector $\boldsymbol{E}$ are then obtained from (3.9), using (3.2)–(3.7), and a correction vector $\boldsymbol{\Delta}$ is next computed by Newton's method,

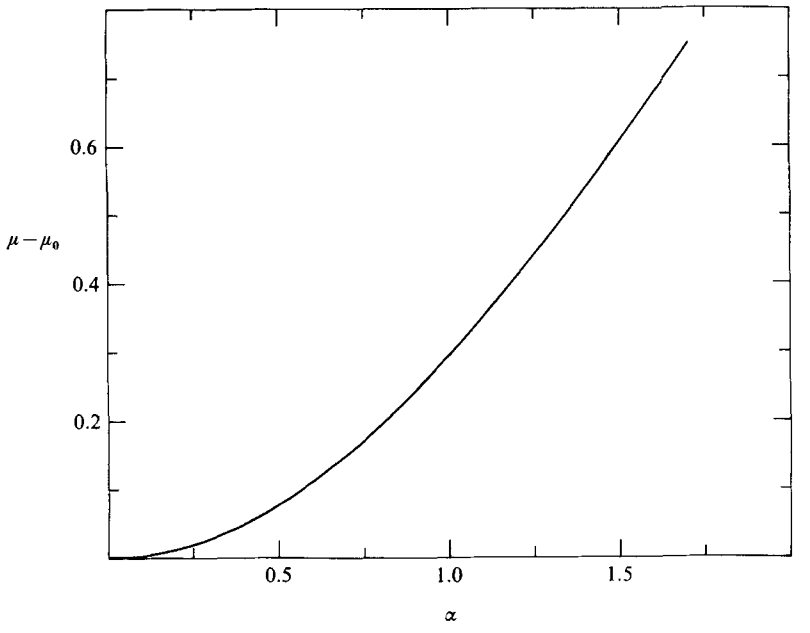

FIGURE 1. Wave-speed parameter as a function of α for $H = 0.005$, $K = 0.4$, $d_M = 0.9$.

as the solution to the matrix equation

$$J(\boldsymbol{u})\,\boldsymbol{\Delta} = -\boldsymbol{E}(\boldsymbol{u}), \tag{3.11}$$

in which $J(\boldsymbol{u})$ is the Jacobian matrix of derivatives of the components of the error vector $\boldsymbol{E}$. Finally, a new estimate $\boldsymbol{u}$ of the solution is obtained by adding the vector $\boldsymbol{\Delta}$ to the previous estimate $\boldsymbol{u}$. If the new vector $\boldsymbol{u}$ is a *worse* approximation to the solution of (3.8) than before, in the sense that the norm $(\boldsymbol{E}^{\mathrm{T}}\boldsymbol{E})^{\frac{1}{2}}$ is *increased* rather than decreased, then the correction step $\boldsymbol{\Delta}$ is halved and a new estimate $\boldsymbol{u}$ formed. This simple modification to Newton's method is of great importance in obtaining large-amplitude solutions to the present problem. The derivatives in the Jacobian matrix J in (3.11) are evaluated using forward differences.

4. Presentation of results

Solutions for pure gravity waves may be obtained by setting $K = 0$ in our numerical scheme, and provide a check on the correctness of our method. Computed values of the wave-speed parameter μ are in excellent agreement with the results tabulated by Cokelet (1977), and with those presented in Paper 1. When $N = 101$, waves up to 95% of the theoretical maximum height may be computed, after which Newton's method does not yield further solutions owing to the increasingly slow convergence of the Fourier series (3.2) with increasing wave amplitude α. At every value of the flexural rigidity K, internal checks on the accuracy of the solutions are performed, such as comparing results obtained with different numbers of Fourier coefficients N and grid-points Q, and monitoring the accuracy to which (2.7) and (2.8) are satisfied.

In figure 1 we present the difference between the wave-speed parameter μ and the linearized value μ_0 (given in (3.10)) as a function of the half-wave height α, for the

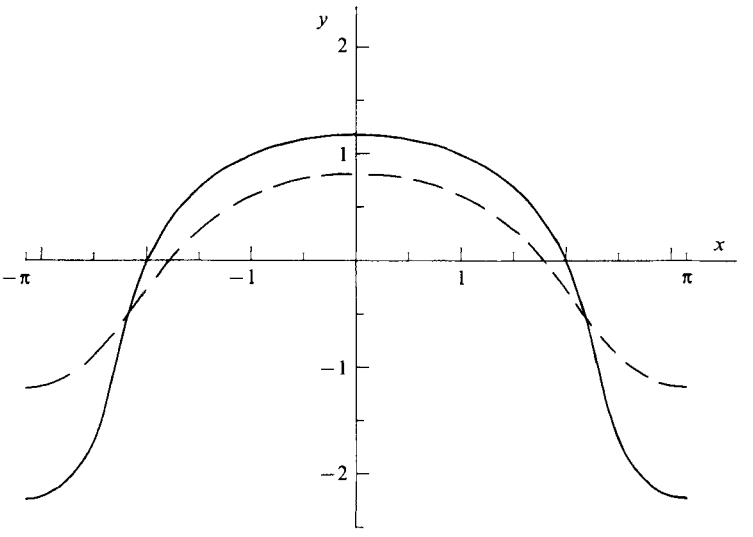

FIGURE 2. Wave profiles for $H = 0.005$, $K = 0.4$, $d_M = 0.9$ at the two values of half-wave height $\alpha = 1$ (– – –) and $\alpha = 1.7$ (——). The scale is the same on the vertical and horizontal axes.

case $H = 0.005$, $K = 0.4$, $d_M = 0.9$. A similar graph was presented in Paper 1, but there it was found that the series solution predicted a singularity in the wave speed at about $\alpha = 0.126$. Our numerical results are in good agreement with those obtained by the series method for $\alpha \lesssim 0.12$, but do not detect any such singular behaviour at these small values of α. In Paper 1, the singularity predicted by the series method to occur at about $\alpha = 0.126$ was presumed to correspond to the failure of the mathematical model, perhaps due to crack formation in the floating elastic sheet. This interpretation was based upon the view, sometimes advanced in the literature (see, for example, Van Dyke 1974), that a singularity on the positive real axis of the expansion variable in a series solution indicates either that the mathematical model ceases to describe the physical phenomenon at this point, or that the solution becomes a multiple-valued function of the expansion variable through the formation of square-root-type singularities. Figure 1, however, shows that neither of these possibilities occurs near $\alpha = 0.126$, and so the conjecture in Paper 1 that the elastic sheet might in practice crack at this value of half-wave height must be incorrect. Instead, it now appears that the singularity at $\alpha = 0.126$ predicted by the series method indicates a narrow region of nonlinear resonance, as in the model problem discussed by Roberts (1981). This will be discussed more fully later.

Figure 1 indicates that solutions may be obtained at extremely large values of the half-wave height α when $K = 0.4$, and it was not until the value $\alpha = 1.7$ was reached that the Newton's-method solution suddenly failed to continue to larger wave heights. The reason for the failure of Newton's method to continue past $\alpha = 1.7$ is presently not understood, although it is possible that the wave speed might become a multi-valued function of α, as occurred in the studies of interfacial waves undertaken by Turner & Vanden-Broeck (1986) and Grimshaw & Pullin (1986).

Wave profiles are shown in figure 2 for the case $H = 0.005$, $K = 0.4$, $d_M = 0.9$ and the two values $\alpha = 1$ and $\alpha = 1.7$ of the half-wave height. The scale is the same on both the vertical and horizontal axes, so that the profiles in figure 2 are as would actually be observed. The wave shape is markedly different from that of gravity waves, however, since large waves ultimately develop very flat crests and rather

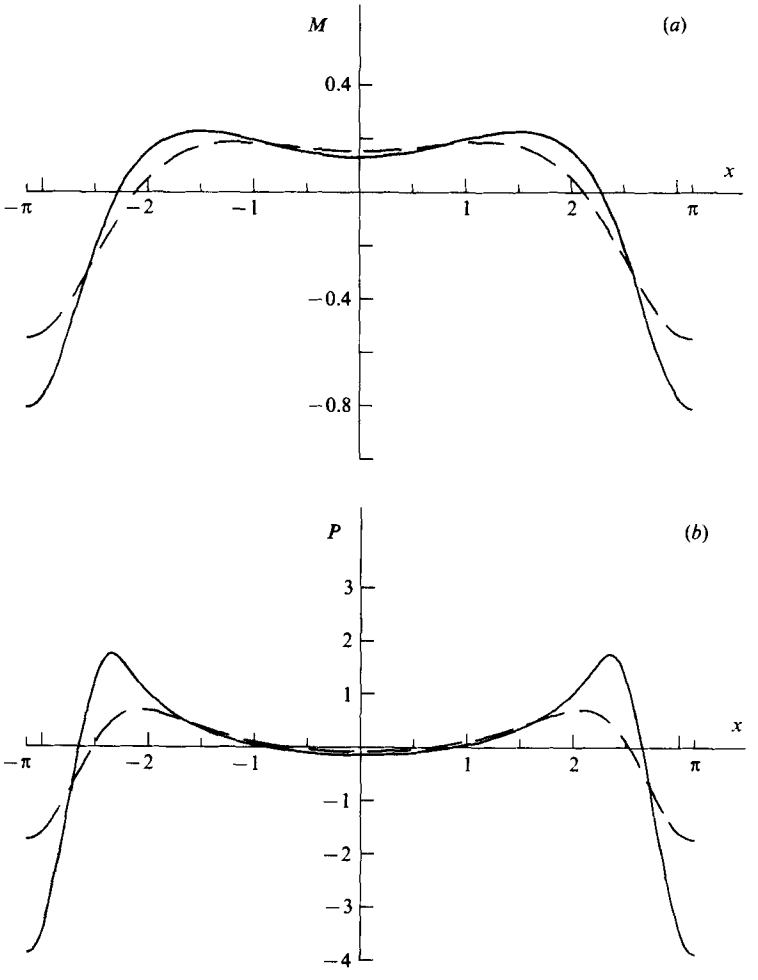

FIGURE 3. (*a*) Bending moment and (*b*) pressure profiles on the bottom face of the elastic sheet for $H = 0.005$, $K = 0.4$, $d_M = 0.9$ at $\alpha = 1$ (– – –) and $\alpha = 1.7$ (——).

narrow troughs. In fact, the wave profiles in figure 2 are similar to the interfacial-wave shapes presented by Grimshaw & Pullin (1986), and it is perhaps possible that S-shaped, or 'over-hanging', portions may develop in the wave profiles of the present problem also.

In keeping with Paper 1, we show in figure 3(*a*, *b*) the moment M and pressure P for the two waves in figure 2 as functions of x. As the wave amplitude α increases, the moment profile ultimately develops a weak local minimum at $x = 0$, and large negative values at the wave troughs $x = \pm\pi$. Equation (2.6) shows that the bending moment M is proportional to the curvature of the centreplane of the elastic sheet, and figure 3(*a*) thus indicates that the curvature of the surface at the wave troughs is large. In practice, such large curvatures could result in cracking of the elastic sheet near these points. The pressure profiles in figure 3(*b*) likewise show large negative values in these regions, and an additional interval of small negative pressures near $x = 0$. For the wave obtained with $\alpha = 1.7$, sharp pressure maxima have developed near the points $x = \pm 2.35$.

Figure 4 shows the difference between the wave-speed parameter μ and the

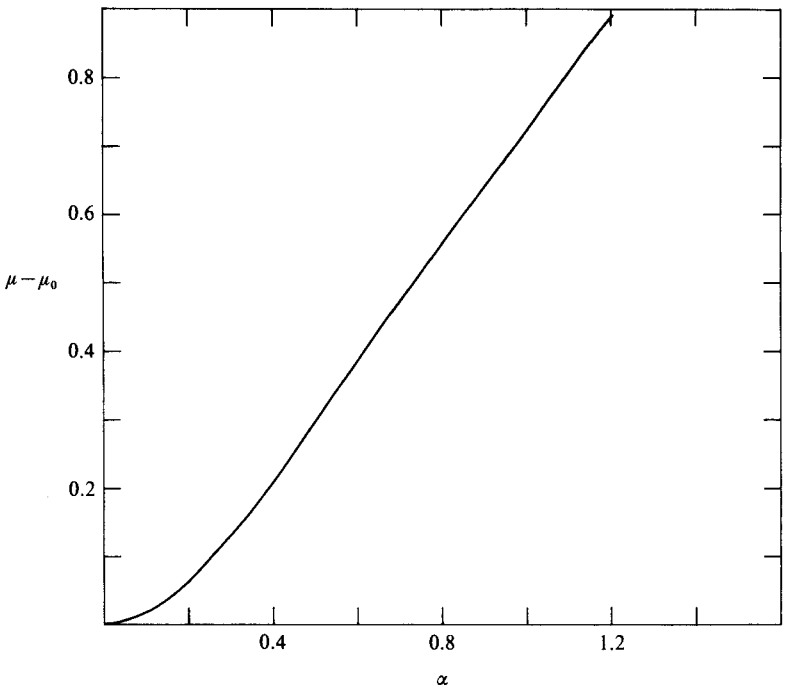

FIGURE 4. Wave-speed parameter as a function of α for $H = 0.005$, $K = 0.05$, $d_M = 0.9$.

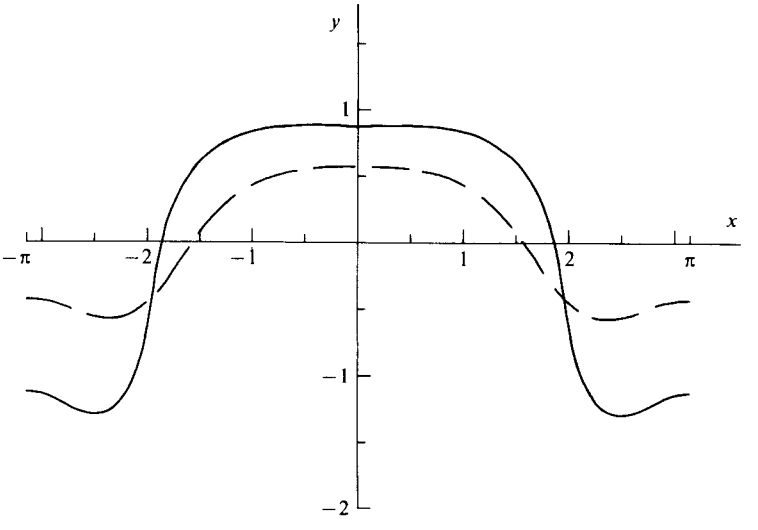

FIGURE 5. Wave profiles for $H = 0.005$, $K = 0.05$, $d_M = 0.9$ at the two values of half-wave height $\alpha = 0.5$ (----) and $\alpha = 1$(——).

linearized value μ_0 in (3.10) as a function of half-wave height α, for the case $H = 0.005$, $K = 0.05$, $d_M = 0.9$. The series method of Paper 1 again predicted a singularity in wave speed at about $\alpha = 0.107$, but no evidence of this is to be found in figure 4, so that the singularity found by the series method is most likely a point of resonance between different nonlinear solution branches. As indicated in figure 4, solutions have been found for half-wave heights as large as $\alpha = 1.2$; there is every indication that solutions for larger α could be obtained, although to do so would

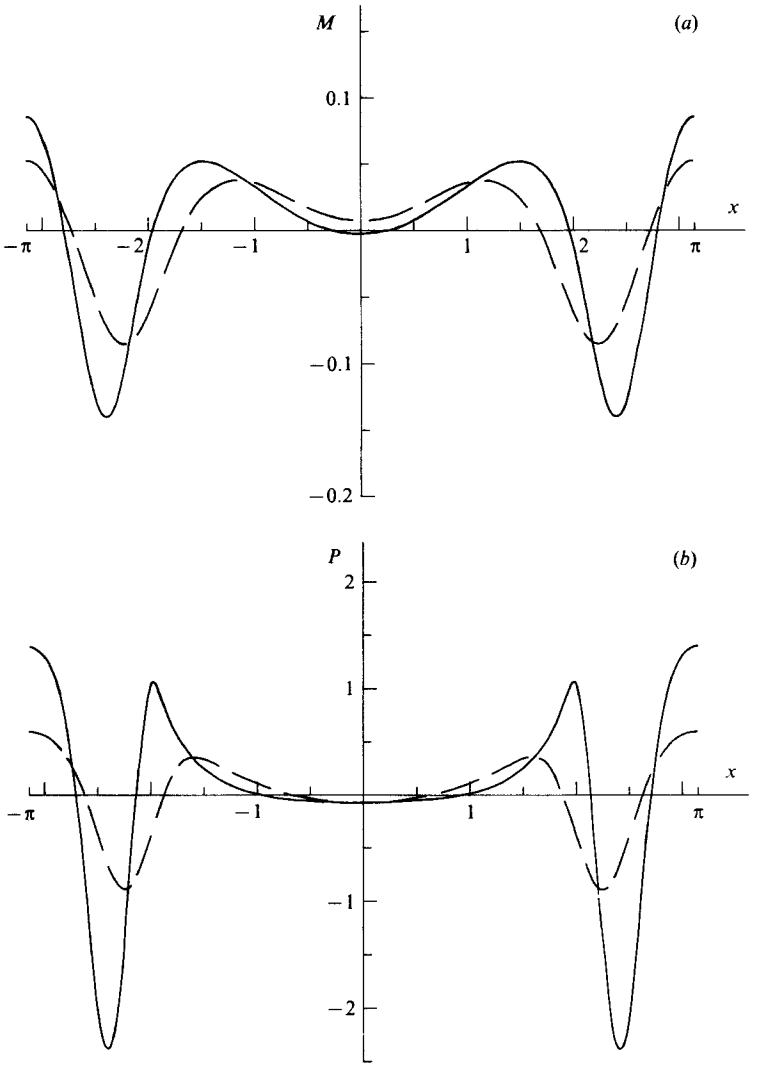

FIGURE 6. (*a*) Bending moment and (*b*) pressure profiles on the bottom face of the elastic sheet for $H = 0.005$, $K = 0.05$, $d_{\mathrm{M}} = 0.9$ at $\alpha = 0.5$ (– – –) and $\alpha = 1$ (——).

require excessive amounts of computer time, since for $K = 0.05$, the convergence of Newton's method becomes very slow as α is increased.

Two wave profiles are shown for this case ($H = 0.005$, $K = 0.05$, $d_{\mathrm{M}} = 0.9$) in figure 5, at the two values of half-wave height $\alpha = 0.5$ and $\alpha = 1$. It was proved in Paper 1 that the series method of solution used there would fail at the singular values

$$d_{\mathrm{M}} K = \frac{1}{n(n^2+n+1)}, \quad n = 2, 3, 4, \ldots \tag{4.1}$$

and since the value $d_{\mathrm{M}} K = 0.045$ used in figures 4 and 5 lies between the first two critical points $\frac{1}{14}$ and $\frac{1}{39}$, a different branch of the solution is expected from that shown in figures 1–3 ($K = 0.4$). Indeed, an immediate qualitative difference is evident between the waves in figure 5 ($K = 0.05$) and those in figure 2 ($K = 0.4$), since in figure 5 both waves possess an extra 'dimple' near the wave trough. In addition,

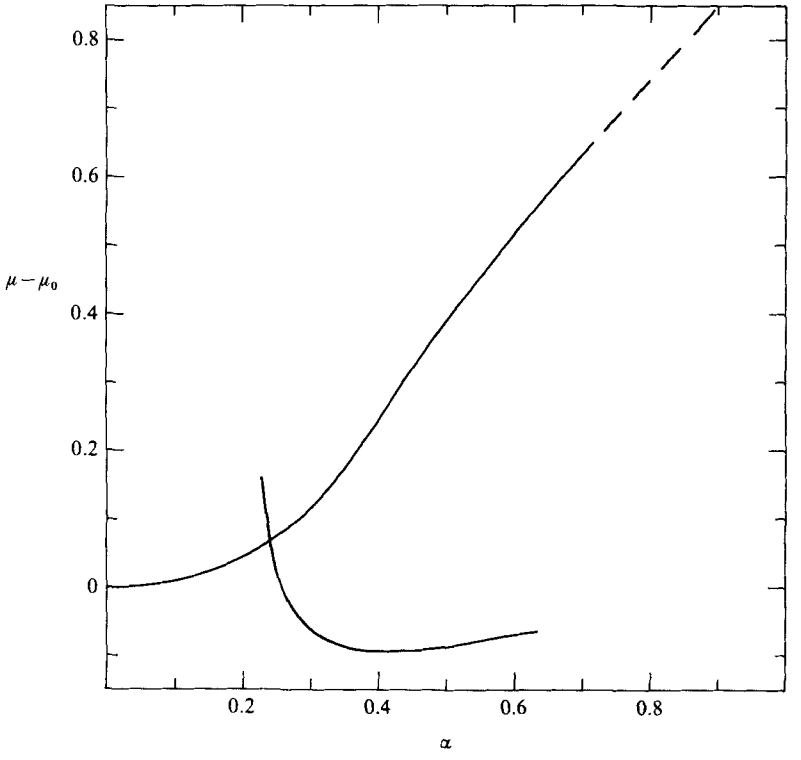

FIGURE 7. Wave-speed parameter as a function of α for $H = 0.005$, $K = 0.009$, $d_M = 0.9$.

there is actually a very weak local minimum in the wave profile for $\alpha = 1$ at $x = 0$, although this may be too slight to be visible in figure 5.

In figure 6(a, b), moment and pressure profiles are shown for the two waves in figure 5. Both profiles show an extra local maximum to the corresponding profiles for $K = 0.4$ displayed in figure 3, as was reported previously in Paper 1. However, in Paper 1 it was supposed that these extra 'dimples' would not be seen in the wave profile itself; this supposition is obviously incorrect, as figure 5 makes clear, and is a consequence of the fact that the series method is incapable of continuing to large enough amplitudes for the dimples in the wave profiles to become visible.

Figure 7 shows the difference between the wave-speed parameter μ and the linearized value μ_0 as a function of α for the case $H = 0.005$, $K = 0.009$, $d_M = 0.9$. This was the most accurate of the cases discussed in Paper 1, where it was found that the series method unambiguously indicated a pole singularity in the wave speed at $\alpha = 0.100073$. In fact, the series method of Paper 1 was capable of analytically continuing the wave speed past this pole singularity, although the results obtained with $\alpha > 0.100073$ were dismissed as 'physically meaningless', which is almost certainly not the case. Instead, the series method jumps from one branch of the solution to another at $\alpha = 0.100073$, similar to its behaviour in a recent study of the forced Duffing equation, undertaken by Forbes (1987).

When $K = 0.009$, the Newton's-method solution converged to two different solution branches, portions of which are sketched in figure 7. On the upper branch, for which $\mu - \mu_0 > 0$, it was found possible to compute accurate solutions at least in the interval $0 < \alpha < 0.7$; solutions for larger α could also be obtained at the expense of an extraordinarily large number of iterations of Newton's method, and

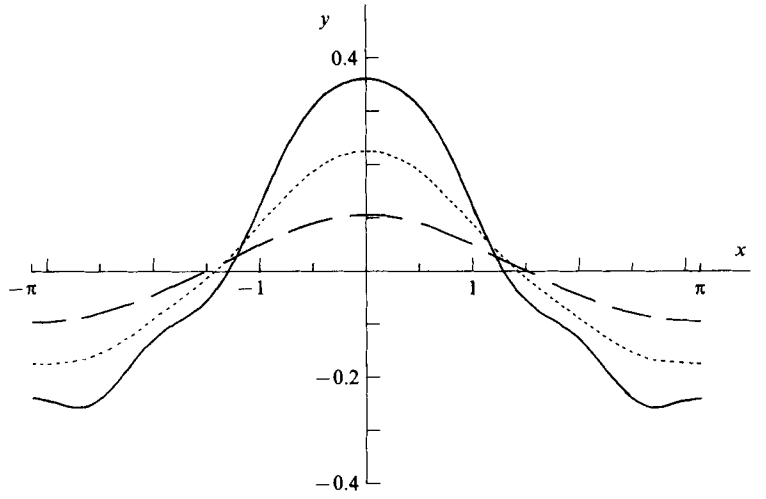

FIGURE 8. Wave profiles for $H = 0.005$, $K = 0.009$, $d_M = 0.9$ at the three values of half-wave height $\alpha = 0.1$ (– – –), $\alpha = 0.2$ (·····) and $\alpha = 0.3$ (——).

consequently large amounts of computer run time. Some of these results are of uncertain accuracy, and have been sketched with a dashed line in figure 7. The lower solution branch was obtained by starting at $\alpha = 0.6$ with the initial guess for Newton's method supplied by the linearized solution (3.10), and then decreasing α incrementally, using the previous solution as a starting guess for the new value of α. Solutions were obtained in this way down to $\alpha = 0.25$; thereafter, an 'inverse' numerical method was employed, whereby μ is prescribed in advance and α determined as an unknown constant. This technique enabled the lower branch of solutions to be continued down until about $\alpha = 0.227$, when the slow convergence of Newton's method and mounting costs of computer time prevented solutions at smaller values of α from being obtained.

As the lower branch of solutions in figure 7 is continued to smaller α, it is observed that the wave-speed parameter μ increases abruptly, so that the lower branch appears to intersect the upper branch at about $\alpha = 0.24$ ($\mu - \mu_0 = 0.069$). In an attempt to determine whether this point represents a true bifurcation, we have monitored the determinant of the Jacobian matrix in Newton's method whilst proceeding along a particular solution branch. As indicated by Chen & Saffman (1980), a vanishing determinant would indicate that the two branches actually intersected at such a point, establishing the presence of a bifurcation.

Our results show that the determinant of the Jacobian matrix does not change sign nor does it appear to become zero on passing through the apparent intersection point of the two branches shown in figure 7. Evidently this point is not a simple bifurcation point, and there is no numerical evidence to suggest that the two different branches in figure 7 intersect at all, in spite of the fact that the values of μ coincide for one value of α. It therefore seems likely that the two solution branches in figure 7 remain distinct at the cross-over point $\alpha \approx 0.24$. However, the possibility of a further resonance in a narrow interval about this point cannot yet be dismissed, and the series method of Paper 1 in fact detected such a phenomenon at $\alpha = 0.100073$. These observations suggest that a large number of different solution branches exists, although our numerical methods have so far only detected two.

Three wave profiles are displayed in figure 8, for the case $H = 0.005$, $K = 0.009$,

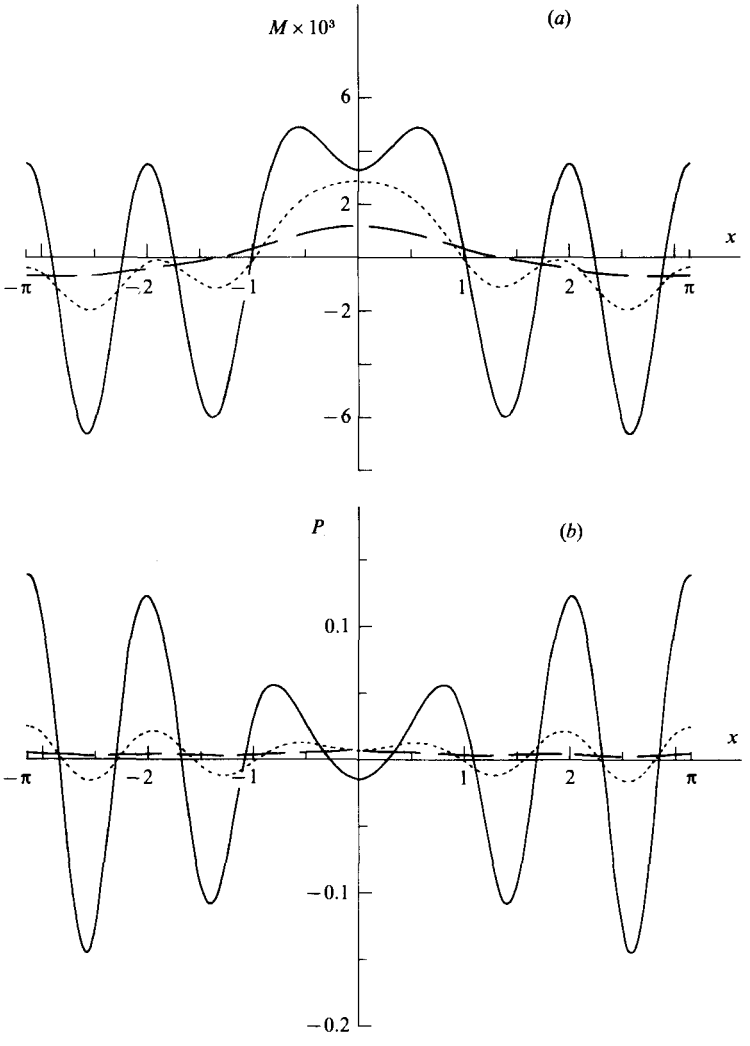

FIGURE 9. (*a*) Bending moment and (*b*) pressure profiles on the bottom face of the elastic sheet for $H = 0.005$, $K = 0.009$, $d_M = 0.9$ at $\alpha = 0.1$ (– – –), $\alpha = 0.2$ (·····) and $\alpha = 0.3$ (——).

$d_M = 0.9$, at the half-wave heights $\alpha = 0.1$, 0.2 and 0.3. These all belong to the upper solution branch in figure 7, and the wave shape for $\alpha = 0.1$ is graphically indistinguishable from that obtained by the series method in Paper 1 for the same value of α. As the wave amplitude is increased, additional maxima and minima appear in the wave profiles, and these are clearly visible in the region of the troughs, for the solution obtained with $\alpha = 0.3$.

Moment and pressure profiles for the three waves in figure 8 are shown in figure 9 (*a*, *b*). Notice that the pressure profile for $\alpha = 0.1$ in figure 9 (*b*) does not possess the exaggerated minimum at $x = 0$ that was predicted by the series method in Paper 1. Both profiles in figure 9 possess many secondary maxima and minima.

In figure 10, two different solutions are presented for the case $H = 0.005$, $K = 0.009$, $d_M = 0.9$ at the same value $\alpha = 0.4$ of the half-wave height. The wave sketched with a solid line belongs to the upper branch of solutions in figure 7, and its wave-speed parameter is $\mu = 1.251\,563$. The secondary wavelet near the troughs is

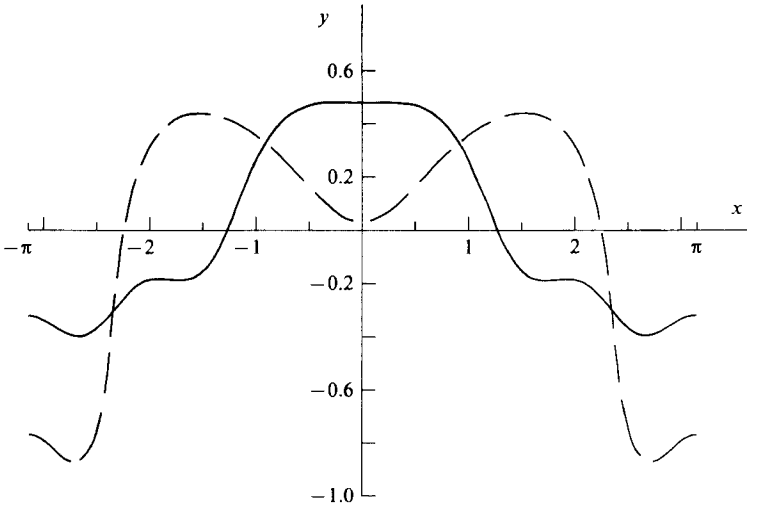

FIGURE 10. Two different solutions for $H = 0.005$, $K = 0.009$, $d_M = 0.9$ and $\alpha = 0.4$. Shown are a slow-wave (– – –) and a fast-wave (——) solution.

now well developed, and there is also a weak local minimum at $x = 0$, although this is too small to be seen from figure 10. The solution sketched with a dashed line belongs to the portion of the lower branch of solutions in figure 7, and its wave speed is $\mu = 0.9130585$. In addition to a small 'dimple' near each trough, there is also a pronounced local minimum at $x = 0$. The difference between the highest and lowest points on the wave profile is much greater for the lower-branch solution in figure 10 than for the upper-branch solution, and in practice one might expect such large slow waves to be unstable.

In Paper 1 it was demonstrated that the series-solution technique failed at the singular values of flexural rigidity given in (4.1). At the first resonance value $d_M K = \frac{1}{14}$ (with $n = 2$), *two* separate solutions were computed by means of a low-order perturbation expansion, showing that the singular values of K in (4.1) are associated with the existence of multiple solutions. This is confirmed in figure 11, where two distinct solutions are given for the case $H = 0.005$, $\alpha = 0.5$, $d_M = 0.9$ with $d_M K = \frac{1}{14}$. The wave drawn with a solid line is the faster of the two, and has speed $\mu = 1.490692$. It was obtained using as a starting guess for Newton's method the values $\mu = \mu_0 + \frac{1}{2}\alpha$, $A_0 = 0$, $A_1 = \alpha$, $A_2 = \frac{1}{2}\alpha$, $A_3 = \ldots = A_N = 0$; these values are an approximation to the upper-branch solution computed in Paper 1. This profile possesses a local minimum in the vicinity of the wave troughs. The other solution, sketched with a dashed line in figure 11, has wave speed $\mu = 0.9567068$ and was obtained using the linearized solution (3.10) as the starting guess for Newton's method. It possesses a weak local minimum at $x = 0$.

We conclude this exposition of the numerical results with a brief discussion of the effects of altering the sheet thickness H, hitherto maintained constant. Figure 12 is a plot of $\mu - \mu_0$ against the sheet thickness H for the case $\alpha = 0.5$, $K = 0.4$, $d_M = 0.9$. The wave-speed parameter μ increases almost linearly, although with an additional small upward inflexion, until the value $H = 4.7$ is reached, beyond which point Newton's method suddenly fails to converge. The precise mathematical nature of the apparent singularity near $H = 4.7$ is presently not understood, in particular since the Fourier series are highly convergent at $H = 4.7$, although it is intuitively clear that

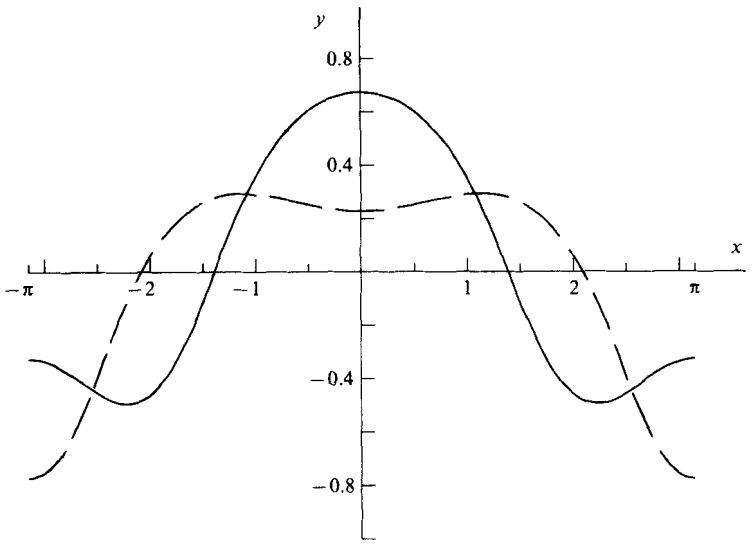

FIGURE 11. Two different solutions at the singular point $d_M K = \frac{1}{14}$, for $H = 0.005$, $\alpha = 0.5$, $d_M = 0.9$. Shown are a slow-wave (– – –) and a fast-wave (——) solution.

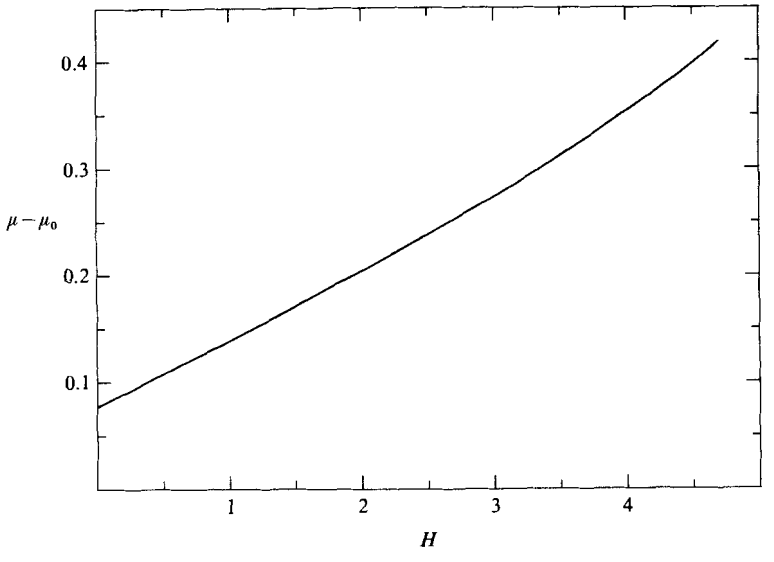

FIGURE 12. Wave-speed parameter as a function of H for $\alpha = 0.5$, $K = 0.4$, $d_M = 0.9$.

there must ultimately cease to be solutions for sufficiently large H in figure 12. This is because, as pointed out in Paper 1, the Bernoulli equation (2.8) reduces to that describing pure gravity waves as $H \to \infty$, so that these are the only possible outcome for large H. Since the value $\alpha = 0.5$ of half-wave height assumed in figure 12 exceeds the maximum value $\alpha = 0.443\,13$ for pure gravity waves (taken from Cokelet 1977), then the solution branch in figure 12 must terminate at some finite H.

Two wave profiles are shown in figure 13, for the case $\alpha = 0.5$, $K = 0.4$, $d_M = 0.9$. The dashed line indicates the shape of a wave beneath a floating elastic sheet of zero thickness, and the solid line represents the wave profile of the near-limiting wave for which $H = 4.7$. As H is increased, it is clear that the wave begins to develop the

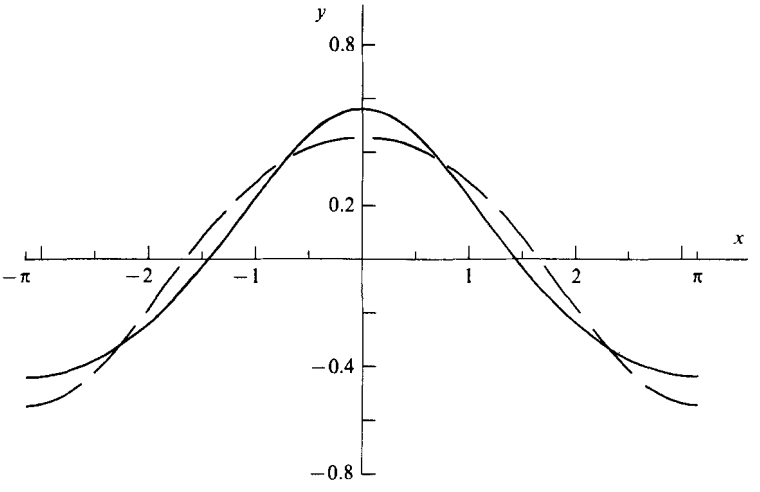

FIGURE 13. Wave profiles for $\alpha = 0.5$, $K = 0.4$, $d_M = 0.9$ at the two values of sheet thickness $H = 0$ (– – –) and $H = 4.7$ (——).

characteristic peaked crests and broad, flat troughs associated with pure gravity waves of large amplitude.

5. Summary and discussion

The equations of motion, derived in Paper 1, which describe the shape of two-dimensional waves beneath a floating elastic sheet have been solved accurately in the present paper using a Galerkin-type method. The prediction of Paper 1 that, for small wave amplitude, a different nonlinear branch of the solution is obtained in each of the intervals

$$0 < d_M^{-1} K^{-1} < 14$$

and

$$n(n^2+n+1) < d_M^{-1} K^{-1} < (n+1)(n^2+3n+3), \quad n = 2, 3, 4, \ldots$$

appears to be confirmed in the present paper. These different solution branches are characterized by different numbers of 'dimples' in the wave profile, analogous to the case of capillary–gravity waves investigated by Schwartz & Vanden-Broeck (1979), for example. Different numbers of subsidiary maxima and minima are also present in the moment and pressure profiles, and in Paper 1 it was erroneously suggested that these were the only distinguishing features between the various solution branches, since the series method of Paper 1 was not capable of continuing to large enough wave height for the dimples in the wave profile itself to become visible.

For each value of the flexural rigidity investigated, waves of very large height were computed. This disproves the conjecture in Paper 1 that the waves should be limited to rather modest heights by the presence of a singularity predicted by the series method; instead, this singularity in the series method is now believed to correspond to a narrow region of nonlinear resonance, at which the series method jumps from one solution branch to another.

Multiple solutions have been computed for certain values of the flexural rigidity K, confirming the predictions of Paper 1. Other solution branches could presumably also be obtained at the same values of K using the present numerical scheme, simply by altering the initial guess supplied to Newton's method in some appropriate manner.

The stability of these branches has not been investigated, however, and it is possible that some of the solutions presented here may be unstable. To the extent that our numerical scheme does not solve directly for the wave profile, but instead determines the coefficients of its Fourier expansion, the method should be capable of computing unstable solutions.

With $K = 0.4$, extremely large waves have been computed, for which the wave height exceeds half the wavelength. There is apparently a maximum wave height beyond which solutions cannot be obtained, however, and it may be of mathematical interest to examine the nature of the limiting behaviour near this maximum height. It is possible that the wave speed may become a double-valued function of half-wave height, with S-shaped portions appearing in the wave profile, as occurs in the study of interfacial gravity waves reported by Turner & Vanden-Broeck (1986) and Grimshaw & Pullin (1986), for example. From a practical point of view, however, these considerations are possibly of limited interest, since it is surely to be expected that our simple description of the behaviour of the elastic sheet, although nonlinear, will not adequately model the sheet response to the extreme deflections encountered in this study. More complete descriptions of the sheet behaviour are presently under investigation.

As indicated in the introduction, the initial motivation for studying this problem was to provide a description of waves beneath a floating ice sheet. The present model undoubtedly does this for waves of sufficiently small amplitude, although the extremely large-amplitude solutions encountered here are not expected to be relevant to the behaviour of ice. Instead, the large curvatures and pressures developed near the wave troughs would cause cracking to occur, resulting in the formation of floating blocks of ice.

I am grateful to a referee for valuable remarks concerning the results presented in figure 7.

REFERENCES

CHEN, B. & SAFFMAN, P. G. 1980 Numerical evidence for the existence of new types of gravity waves of permanent form on deep water. *Stud. Appl. Maths* **62**, 1–21.

COKELET, E. D. 1977 Steep gravity waves in water of arbitrary uniform depth. *Phil. Trans. R. Soc. Lond.* A **286**, 183–230.

FORBES, L. K. 1986 Surface waves of large amplitude beneath an elastic sheet. Part 1. High-order series solution. *J. Fluid Mech.* **169**, 409–428.

FORBES, L. K. 1987 Periodic solutions of high accuracy to the forced Duffing equation: Perturbation series in the forcing amplitude. *J. Austral. Math. Soc.* B **29**, 21–38.

GRIMSHAW, R. H. J. & PULLIN, D. I. 1986 Extreme interfacial waves. *Phys. Fluids* **29**, 2802–2807.

HOGAN, S. J. 1980 Some effects of surface tension on steep water waves. Part 2. *J. Fluid Mech.* **96**, 417–445.

HOGAN, S. J. 1981 Some effects of surface tension on steep water waves. Part 3. *J. Fluid Mech.* **110**, 381–410.

HOLYER, J. Y. 1979 Large amplitude progressive interfacial waves. *J. Fluid Mech.* **93**, 433–448.

PULLIN, D. I. & GRIMSHAW, R. H. J. 1983 Nonlinear interfacial progressive waves near a boundary in a Boussinesq fluid. *Phys. Fluids* **26**, 897–905.

RIENECKER, M. M. & FENTON, J. D. 1981 A Fourier approximation method for steady water waves. *J. Fluid Mech.* **104**, 119–137.

ROBERTS, A. J. 1981 The behaviour of harmonic resonant steady solutions to a model differential equation. *Q. J. Mech. Appl. Maths* **34**, 287–310.

ROBERTS, A. J. 1983 Highly nonlinear short-crested water waves. *J. Fluid Mech.* **135**, 301–321.

SCHWARTZ, L. W. 1974 Computer extension and analytic continuation of Stokes' expansion for gravity waves. *J. Fluid Mech.* **62**, 553–578.

SCHWARTZ, L. W. & FENTON, J. D. 1982 Strongly nonlinear waves. *Ann. Rev. Fluid Mech.* **14**, 39–60.

SCHWARTZ, L. W. & VANDEN-BROECK, J.-M. 1979 Numerical solution of the exact equations for capillary–gravity waves. *J. Fluid Mech.* **95**, 119–139.

STOKES, G. G. 1880 *Mathematical and Physical Papers*, vol. 1. Cambridge University Press.

TURNER, R. E. L. & VANDEN-BROECK, J.-M. 1986 The limiting configuration of interfacial gravity waves. *Phys. Fluids* **29**, 372–375.

VAN DYKE, M. D. 1974 Analysis and improvement of perturbation series. *Q. J. Mech. Appl. Maths* **27**, 423–450.

WILTON, J. R. 1915 On ripples. *Phil. Mag.* **29**, 688–700.